NACA

CASE FILE
COPY

RESEARCH MEMORANDUM

EXPERIMENTAL INVESTIGATION OF A TRANSONIC COMPRESSOR

ROTOR WITH A 1.5-INCH CHORD LENGTH AND AN ASPECT

RATIO OF 3.0

II - BLADE-ELEMENT PERFORMANCE

By Francis C. Schwenk and Edward R. Tysl

Lewis Flight Propulsion Laboratory
Cleveland, Ohio

NATIONAL ADVISORY COMMITTEE
FOR AERONAUTICS
WASHINGTON
August 18, 1955

NATIONAL ADVISORY COMMITTEE FOR AERONAUTICS

RESEARCH MEMORANDUM

EXPERIMENTAL INVESTIGATION OF A TRANSONIC COMPRESSOR ROTOR WITH A

1.5-INCH CHORD LENGTH AND AN ASPECT RATIO OF 3.0

II - BLADE-ELEMENT PERFORMANCE

By Francis C. Schwenk and Edward R. Tysl

SUMMARY

A transonic compressor rotor with double-circular-arc blade sections was designed and tested to investigate the aerodynamic effects of using a short blade chord and a high aspect ratio. This report presents the blade-element performance and performance analysis. The design total-pressure ratio of this rotor was 1.35 at a corrected specific weight flow of 31.3 pounds per second per square foot of frontal area with the rotor operating at a corrected tip speed of 1000 feet per second.

A sharp increase in blade-element losses near the tip of the rotor was noted as speed increased from 90 to 100 percent of corrected design speed. This increase in loss was mainly attributed to blade loading and not to excessive shock losses.

There was good agreement for all speeds at the tip and mean sections between measured deviation angles at minimum-loss incidence angle and deviation angles determined by Carter's rule.

A simplified-radial-equilibrium calculation for design speed was made at the rotor outlet to determine if the method was applicable for this design. Except for radii near the hub, comparison of the calculated and measured static pressures indicated good agreement at the lower weight flows. At the high weight flow, agreement near the hub was better than that experienced at the lower weight flows; however, there was a slight deviation between the two values near the tip section.

The use of a short chord length and high aspect ratio in this type of transonic compressor design caused no serious problems in performance for the Reynolds number and Mach number levels encountered in these tests.

INTRODUCTION

A transonic compressor rotor with double-circular-arc blade sections has been designed and tested at the NACA Lewis laboratory to investigate the aerodynamic effect of using short chord lengths for relative inlet Mach numbers up to 1.15. Reference 1 describes the 1.5-inch-chord rotor used in this investigation. It also contains the design procedure, mass-averaged over-all performance, radial variations of rotor-inlet and -outlet conditions, and rotating-stall characteristics.

This report extends the results and analysis given in reference 1 and provides more details on the operation of this compressor rotor. This information is provided by presenting the blade-element characteristics. The blade-element results also add to the available design data for the use of double-circular-arc airfoils in compressor rotors.

Measured radial variations of rotor-outlet static pressure are compared with the static pressure computed from the simplified-radial-equilibrium equation. This concept is one of the bases for current compressor design procedures and under some circumstances may require alteration for compressors having short chord lengths and high aspect ratios.

For an inlet-stage compressor rotor, the design system may account for the effects of wall boundary layers through the use of a correction factor in the continuity equation. Data on this boundary-layer blockage factor are also presented in this report.

COMPRESSOR DESIGN, APPARATUS, AND TEST PROCEDURE

The 1.5-inch-chord transonic compressor rotor and test rig are described in reference 1. However, it is desirable to restate some of the general design characteristics. These are:

(1) Design total-pressure ratio of 1.35 exclusive of losses in wall boundary-layer regions

(2) Design corrected specific weight flow of 31.3 pounds per second per square foot of frontal area

(3) Design corrected tip speed of 1000 feet per second

(4) Inlet hub-tip radius ratio of 0.5

(5) Aspect ratio of 3.0 resulting from a 1.5-inch chord length and 18-inch tip diameter (rotor-tip solidity is 0.95)

(6) Design adiabatic efficiency of 0.93, computed by use in design of an empirical radial variation of blade-element losses

The mass-averaged performance of this transonic compressor rotor is shown in figure 1.

The geometry of the measured rotor blade elements is given in table I. Figure 2, which is a schematic diagram of the compressor test section, shows the approximate locations of the measuring stations upstream and downstream of the rotor. The instruments and their use are described in reference 1.

The rotor (photograph in fig. 3) was tested over a range of weight flow at 60, 70, 80, 90, and 100 percent of design speed according to the procedure outlined in reference 1.

ROTOR-BLADE-ELEMENT PERFORMANCE

Axial-flow-compressor blades are usually formed by radial stacking of blade profiles or blade elements. These sections lie on assumed stream surfaces of revolution, which are formed by rotating assumed streamlines about the axis of the rotor. To simplify design and analysis of this rotor, the streamlines that lie in the rz-plane (created by the axis of rotation and a radius perpendicular to it) were assumed to be straight lines. They also were assumed to divide the annular passage height into equal-percentage radial increments at the inlet and outlet of this rotor blade.

Blade-element performance of this rotor is presented in figure 4 for five speeds at three blade-element sections. These sections are located at 84, 50, and 10 percent of the passage height from the outer wall and are called hub, mean, and tip blade elements, respectively. The blade-element characteristics plotted against incidence angle in figure 4 are: relative total-pressure-loss coefficient $\bar{\omega}$; deviation angle δ^0; rotor-inlet relative Mach number M_3'; axial-velocity ratio $V_{z,4}/V_{z,3}$; blade-element loading represented by the diffusion factor D (ref. 2); work coefficient (nondimensional temperature-rise coefficient) $\Delta H/U_t^2$; and blade-element adiabatic efficiency η_b. The calculations and significance of the various parameters in rotor-blade-element analysis are discussed in references 3 and 4. (All symbols used in this report are defined in the appendix.) Reconstruction of velocity diagrams is possible by means of these parameters. The velocity-diagram notation for a blade element is shown in figure 5.

Relative Total-Pressure-Loss Coefficient

The variations of the relative total-pressure-loss coefficient with incidence angle for five speeds and three blade elements are shown in

figure 4. The loss trends are generally similar to previously reported rotor-blade-element data (refs. 3 and 5 to 7) and two-dimensional cascade test results on double-circular-arc airfoils (ref. 8). The variation of the loss coefficient at the hub and mean blade-element sections will be discussed first.

Hub and mean blade elements. - At the hub (fig. 4(a)) in the incidence-angle range investigated, the loss-coefficient level is about the same for all speeds at which this compressor rotor was tested. At the mean section (fig. 4(b)) for incidence angles greater than 6°, there are also only small differences in loss-coefficient level among the various speeds tested. Below incidence angles of 6°, the loss-coefficient level and variation with incidence angle differ with speed or Mach number level. Thus, for the mean section (fig. 4(b)), the low-loss incidence-angle range decreases with increasing Mach number; and the value of the minimum-loss incidence angle becomes greater at the higher speeds. Similar trends have been observed in other rotor tests (refs. 3 and 7). At the hub, the increase in loss coefficient with a decrease in incidence angle was not observed, possibly because the sections were not tested over a wide enough incidence-angle range.

To compare the hub- and mean-section loss levels with past results, loss coefficients in the region of minimum loss taken from faired values of figure 4 are shown in figures 6(a) and (b) plotted against corresponding faired values of diffusion factor D, a blade-element loading parameter (ref. 2). The diffusion factors are well below the limiting value of 0.6 for cascades. The measured hub- and mean-section losses are low and, also, are about equal to low-speed two-dimensional cascade losses (ref. 2). Therefore, it appears that the use of short chord lengths did not cause flow separation and high losses in the hub and mean blade regions in the range of Mach number, Reynolds number, and turbulence level experienced in these tests.

Cascade test results (refs. 9 and 10) show that the losses increase with decreasing Reynolds number in the critical Reynolds number range. For cascades, the critical Reynolds number value (based on chord length) lies somewhere between 1.0×10^5 and 3.0×10^5. The value of critical Reynolds number varies with blade velocity distribution, free-stream turbulence level, and condition of the blade surface. The lowest blade-chord Reynolds numbers for the hub section occurred at 60 percent of design speed. The values of these Reynolds numbers were approximately 2.6×10^5 for an inlet total pressure of 20 inches of mercury absolute. Hub-section Reynolds numbers at design speed were about 3.7×10^5.

Tip blade element. - Figure 4(c) shows the variation of relative total-pressure-loss coefficient with incidence angle for the tip section, which is located about 10 percent of the passage height away from the outer wall.

The loss variations of the tip section of this short-chord rotor follow previously reported data for similar rotor blade sections of longer chord length. At speeds below design (Mach numbers below 1.0), there is little variation in loss level among the various speeds tested. However, at design speed (Mach number of 1.0 or above), the losses are higher than those at the lower speeds. Figure 4(c) also shows an increase in the blade-element loading (diffusion factor D) with an increase in speed. Since the deviation-angle levels (fig. 4(c)) vary only slightly with speed, the changes in diffusion-factor level are caused by the decrease in the axial-velocity ratio with increasing speed (fig. 4(c)).

Both Mach number level and loading can affect the tip-section losses. In previous investigations of transonic compressors (ref. 3 and 5 to 7), values of loss coefficient near minimum loss at each speed were plotted against diffusion factor in an attempt to separate effects of Mach number and loading levels. Figure 6(c) shows such a plot for the tip section of this short-chord rotor along with dashed lines which indicate the range of tip-section data given in reference 2.

The measured losses of this rotor correlate well with previous results. Figure 6(c) indicates that:

(1) Mach number effects (shock losses) on losses were not great enough to cause losses outside the range of values obtained from a number of compressors having conventional (subsonic) tip performance.

(2) Increased blade loading probably accounts for the higher losses at design speed.

Figure 4(c) shows that there is generally an increase in diffusion-factor level with increasing speed; however, the marked change in loss level occurs only for the change in speed from 90 to 100 percent of corrected design speed. No increase in losses with diffusion factor was observed at speeds up to 90 percent of design, because the low-speed diffusion factors were less than 0.4. Reference 2 shows that tip-section losses increase with diffusion factor only when the diffusion factors are greater than 0.35 or 0.40.

The preceding attempt to separate Mach number and loading effects must be qualified because of the wide spread in the correlation data of tip-section loss and diffusion factor given in reference 2 (shown by the dashed lines on fig. 6(c)). The wide spread in the data may indicate that diffusion factor is not the only influence on tip losses, and such effects as tip clearance, casing boundary layer, secondary flow, inlet guide vanes, and so forth, may be the cause of scatter. Until these additional effects can be estimated, it will be difficult to separate and evaluate Mach number and loading effects with any certainty.

Since the measured losses agreed with previous results, it seems that the use of a short chord length in this type of transonic compressor design caused no serious loss problems for the Mach number, Reynolds number, and turbulence levels experienced in these tests. Tip-section Reynolds numbers at design speed were about 5.1×10^5 based on blade chord length.

Reference 1 reports that maximum efficiency at design speed was attained at less than the design corrected specific weight flow of 31.3 pounds per second per square foot of frontal area. At design weight flow, the rotor actually operates in a choked condition as shown in the over-all performance map (fig. 1). The variation of loss coefficient with incidence angle (fig. 4) further illustrates this condition. Operation at design weight flow corresponds to operation at the lowest incidence angles shown on these curves. For the mean and tip sections (figs. 4(b) and (c)), there is evidence of choking as mentioned previously in this report. At this operating point, losses and deviation angles are high, and therefore design work input and pressure ratio were not obtained at design weight flow.

Deviation Angle

If design pressure ratio is to be obtained for a particular blade row, close design control is necessary over the flow direction at the outlet of the blade row. Deviation angle was used as a parameter for outlet flow direction. The deviation angle δ^0 is defined as the angle between the outlet-relative-air-velocity vector and the tangent to the blade mean camber line at the trailing edge (fig. 5). In compressor design, it is also desirable to be able to predict the deviation angle over the range of incidence angle encountered by the rotor.

The variation of measured deviation angle with incidence angle is given in figure 4 for the tip, mean, and hub sections. Above choking incidence angle (lowest value of incidence angle for each speed), deviation angle is independent of speed within a scatter of approximately 1^0 for the tip and mean blade sections. The deviation-angle trend at the mean and tip sections for incidence angles approaching choking values is similar to the loss-coefficient trend with incidence angle in that the measured deviation angles increased with decreasing incidence angles. However, at the hub, the deviation angle continued decreasing with decreasing incidence angle for all speeds.

The measured deviation angles at minimum-loss incidence angles are compared with values obtained from Carter's rule (ref. 11) in figure 7. The deviation angles are plotted against percent design speed merely to catalog the data. Values of the deviation angles (fig. 7) are taken from the faired curves of figure 4 at the minimum-loss incidence angles.

The deviation angles at minimum loss for the tip section agree very well with the values obtained from Carter's rule. The agreement for the

mean section is not quite so good, since the measured values are a little higher. At both tip and mean blade sections (figs. 7(b) and (c)), there is only a small variation of deviation angle with speed over the range of speed investigated. This result agrees with past experience (ref. 4), which has indicated that Mach number level has little effect on the magnitude of the deviation angle for low losses. At the hub section, however, there is an apparent variation in deviation angle with speed. Reexamination of the plot of deviation angle against incidence angle in figure 4(a) indicates a possible reason for this apparent variation. At a fixed angle of incidence, deviation angle tends to increase slightly with an increase in Mach number. In addition, there is an appreciable variation in deviation angle with incidence angle - somewhat greater than expected for a high-solidity section ($\sigma_h = 1.61$) from cascade data. The minimum-loss incidence angle for the hub section also varies a great deal with speed (about 4°). The combination of the aforementioned items could produce the large apparent change in deviation angle with speed at the hub section.

RADIAL EQUILIBRIUM

In current compressor design procedures, the simplified-radial-equilibrium equation is often used to compute the radial static-pressure variation across the passage behind a rotor. The simplified-radial-equilibrium equation

$$\frac{dp}{dr} = \frac{\rho V_\theta^2}{gr} \tag{1}$$

was used to determine the gradient of static pressure across the passage in the design of this rotor (ref. 1). The development of this equation from the equations of motion requires the following assumptions:

(1) The viscous shear forces are negligible.

(2) The flow is axially symmetric.

(3) The radial velocity components are zero.

(4) Radial accelerations due to streamline curvatures in the rz-plane are zero.

In a short-chord, high-aspect-ratio compressor rotor of the type discussed in this report, streamline curvatures could be important. The simplified-radial-equilibrium equation then might not apply in predicting the radial variations of flow conditions at the rotor outlet.

To check the validity of the simplified-radial-equilibrium equation as a design tool, measured static-pressure variations with radius (rotor-

outlet station) are compared with static pressures computed from the
simplified-radial-equilibrium equation in figure 8. Data are given for
three weight flows at design speed.

The static pressures were computed from an integration of equation
(1), following the procedure outlined in reference 3

$$p - p_{ref} = \int_{r_{ref}}^{r} \frac{\rho V_\theta^2}{gr} \, dr \qquad (2)$$

The measured static pressure at the mean radius ($r_4 = 7.00$ in.) was used
as the reference static pressure p_{ref}. The computations employed meas-
ured values of rotor-outlet total pressure, total temperature, and abso-
lute flow angle.

Figure 8 shows that the measured and computed static pressures agree
very well over a portion of the passage for all three weight flows at de-
sign speed. However, the simplified-radial-equilibrium values depart
from the measured values in the tip region for the high weight flow and
in the hub region for the two lower weight flows.

It can be assumed that the preceding departures arise from the pres-
ence of streamline curvature, which is neglected in the calculation of
static-pressure variation with the simplified-radial-equilibrium equa-
tion. Streamline curvatures in this compressor of constant tip diameter
are caused by the combined effects of the hub contour and radial shifts
in the flow as it passes through the rotor. At the two lower flows at
design speed (fig. 8), radial shifts in the flow have little effect and
the hub curvature causes the difference between measured and simplified-
radial-equilibrium static pressures. For the high weight flow, a shift
in the flow toward the hub creates streamline curvatures opposite from
those induced by the hub contour; and a difference between the measured
and computed static pressure appears near the outer wall as shown on
figure 8.

WALL-BOUNDARY-LAYER BLOCKAGE FACTOR

Wall-boundary-layer blockage factor K is defined as the ratio of
actual integrated weight flow to the ideal integrated weight flow (as-
suming no boundary layers). The rotor-inlet and -outlet blockage factors
for this rotor are given in the following table:

$U_t/\sqrt{\theta}$, ft/sec	$W\sqrt{\theta}/\delta A_f$, lb/(sec)(sq ft)	K_4	K_2
800	29.3	0.959	0.988
800	28.9	.956	.998
800	23.1	.945	.989
1000	31.3	.954	.987
1000	30.0	.955	.987
1000	27.8	.937	.988

The design values of 0.985 for K_2 and 0.96 for K_4 were assumed from a previous investigation (ref. 3) which used the same test rig installation.

SUMMARY OF RESULTS

A transonic axial-flow compressor rotor with double-circular-arc airfoil blade sections was designed and tested to investigate the aero-dynamic effects of using short chords and high aspect ratios. The following results were obtained from this experimental investigation of the blade-element performance:

1. The use of a short chord length and high aspect ratio in this type of transonic compressor design caused no serious loss problems for the Reynolds number and turbulence levels experienced in these tests.

2. At the tip section, a sharp increase in relative total-pressure-loss coefficient resulted when speed increased from 90 to 100 percent of corrected design speed. This increase in loss appeared to be caused mainly by blade loading and not by excessive shock losses.

3. Variation in relative total-pressure-loss coefficient with diffusion factor in the low-loss incidence-angle range agreed with results of previous investigations.

4. The deviation angles at the tip section agreed closely with values obtained by Carter's rule. At both tip and mean blade sections, there was very little variation of deviation angle with speed at minimum loss over the speed range investigated.

5. At all radii except near the hub, there was good agreement between measured static pressures and static pressures computed from the simplified-radial-equilibrium equation at design speed for the lower weight flows. However, for the high weight flow at design speed, agreement between the two values of static pressure near the hub improved with a corresponding disagreement near the tip.

Lewis Flight Propulsion Laboratory
        National Advisory Committee for Aeronautics
            Cleveland, Ohio, June 10, 1955

APPENDIX - SYMBOLS

A diagram illustrating the air and blade angles and the velocities is presented in figure 5 to more completely define some of the symbols used.

The following symbols are used in this report:

A_f compressor frontal area based on rotor-tip diameter, 1.767 sq ft

c_p specific heat of air at constant pressure, Btu/(lb)($^\circ$R)

D diffusion factor (ref. 2)

g acceleration due to gravity, 32.17 ft/sec^2

H total enthalpy, $c_p g J T$, sq ft/sec^2

i incidence angle, angle between inlet-relative-air-velocity vector and tangent to blade mean camber line at leading edge, deg

J Joule's constant, 778.26 ft-lb/Btu

K wall-boundary-layer blockage factor

M Mach number

P total pressure, lb/sq ft

p static pressure, lb/sq ft

r radius measured from axis of rotation, in.

T total temperature, $^\circ$R

U blade speed, ft/sec

V air velocity, ft/sec

W weight flow of air, lb/sec

z axis of rotation

β air-flow angle measured from axis of rotation, deg

γ° blade angle, direction of tangent to blade mean camber line at leading or trailing edge, deg

δ ratio of inlet total pressure to NACA standard total pressure, $P_1/2117$

δ^o deviation angle, angle between outlet-relative-air-velocity vector and tangent to blade mean camber line at trailing edge, deg

η adiabatic temperature-rise efficiency

θ ratio of compressor-inlet total temperature to NACA standard temperature, $T_1/518.6$

ρ static density of air, lb/cu ft

σ solidity, ratio of blade chord measured along streamline to average blade spacing

$\overline{\omega}$ relative total-pressure-loss coefficient (ref. 3)

Subscripts:

b   blade element

h   hub of rotor

ref   reference value

t   tip of rotor

z   axial direction

θ tangential direction

1   depression tank

2   upstream of rotor, location of inlet static-pressure rake

3   rotor inlet

4   rotor outlet

Superscript:

'   denotes conditions relative to blade row

REFERENCES

1. Tysl, Edward R., Schwenk, Francis C., and Watkins, Thomas B.: Experimental Investigation of a Transonic Compressor Rotor with a 1.5-Inch Chord Length and an Aspect Ratio of 3.0. I - Design, Over-All Performance, and Rotating-Stall Characteristics. NACA RM E54L31, 1955.

2. Lieblein, Seymour, Schwenk, Francis C., and Broderick, Robert L.: Diffusion Factor for Estimating Losses and Limiting Blade Loadings in Axial-Flow-Compressor Blade Elements. NACA RM E53D01, 1953.

3. Schwenk, Francis C., Lieblein, Seymour, and Lewis, George W., Jr.: Experimental Investigation of an Axial-Flow Compressor Inlet Stage Operating at Transonic Relative Inlet Mach Numbers. III - Blade-Row Performance of Stage with Transonic Rotor and Subsonic Stator at Corrected Tip Speeds of 800 and 1000 Feet Per Second. NACA RM E53G17, 1953.

4. Lieblein, Seymour: Review of High-Performance Axial-Flow-Compressor Blade-Element Theory. NACA RM E53L22, 1954.

5. Sandercock, Donald M., Lieblein, Seymour, and Schwenk, Francis C.: Experimental Investigation of an Axial-Flow Compressor Inlet Stage Operating at Transonic Relative Inlet Mach Numbers. IV - Stage and Blade-Row Performance of Stage with Axial-Discharge Stators. NACA RM E54C26, 1954.

6. Robbins, William H., and Glaser, Frederick W.: Investigation of an Axial-Flow-Compressor Rotor with Circular-Arc Blades Operating up to a Rotor-Inlet Relative Mach Number of 1.22. NACA RM E53D24, 1953.

7. Lewis, George W., Jr., and Schwenk, Francis C.: Experimental Investigation of a Transonic Axial-Flow-Compressor Rotor with Double-Circular-Arc Airfoil Blade Sections. II - Blade-Element Performance. NACA RM E54J08, 1955.

8. Andrews, S. J.: Tests Related to the Effect of Profile Shape and Camber Line on Compressor Cascade Performance. Rep. No. R.60, British N.G.T.E., Oct. 1949.

9. Lawson, T. V.: An Investigation into the Effect of Reynolds Number on a Cascade of Blades with Parabolic Arc Camber Lines. Memo. No. M.195, British N.G.T.E., Nov. 1953.

10. Herrig, Joseph L., Emery, James C., and Erwin, John R.: Systematic Two-Dimensional Cascade Tests of NACA 65-Series Compressor Blades at Low Speeds. NACA RM L51G31, 1951.

11. Carter, A. D. S.: The Low Speed Performance of Related Aerofoils in Cascade. Rep. No. R.55, British N.G.T.E., Sept. 1949.

3693

3693

TABLE I. - MEASURED ROTOR-BLADE-ELEMENT GEOMETRY

Radius, in.		Solidity, σ	Blade inlet angle, γ_3^o, deg	Blade outlet angle, γ_4^o, deg
Inlet, r_3	Outlet, r_4			
9.00	9.00	0.95	----	----
8.54	8.60	1.00	50.6	44.6
8.27	8.36	1.03	49.8	42.8
7.90	8.04	1.07	48.6	40.0
7.49	7.68	1.13	47.1	36.5
6.71	7.00	1.25	44.2	28.9
5.93	6.32	1.40	41.0	20.0
5.15	5.64	1.61	37.7	9.4
4.58	5.00	1.89	----	----
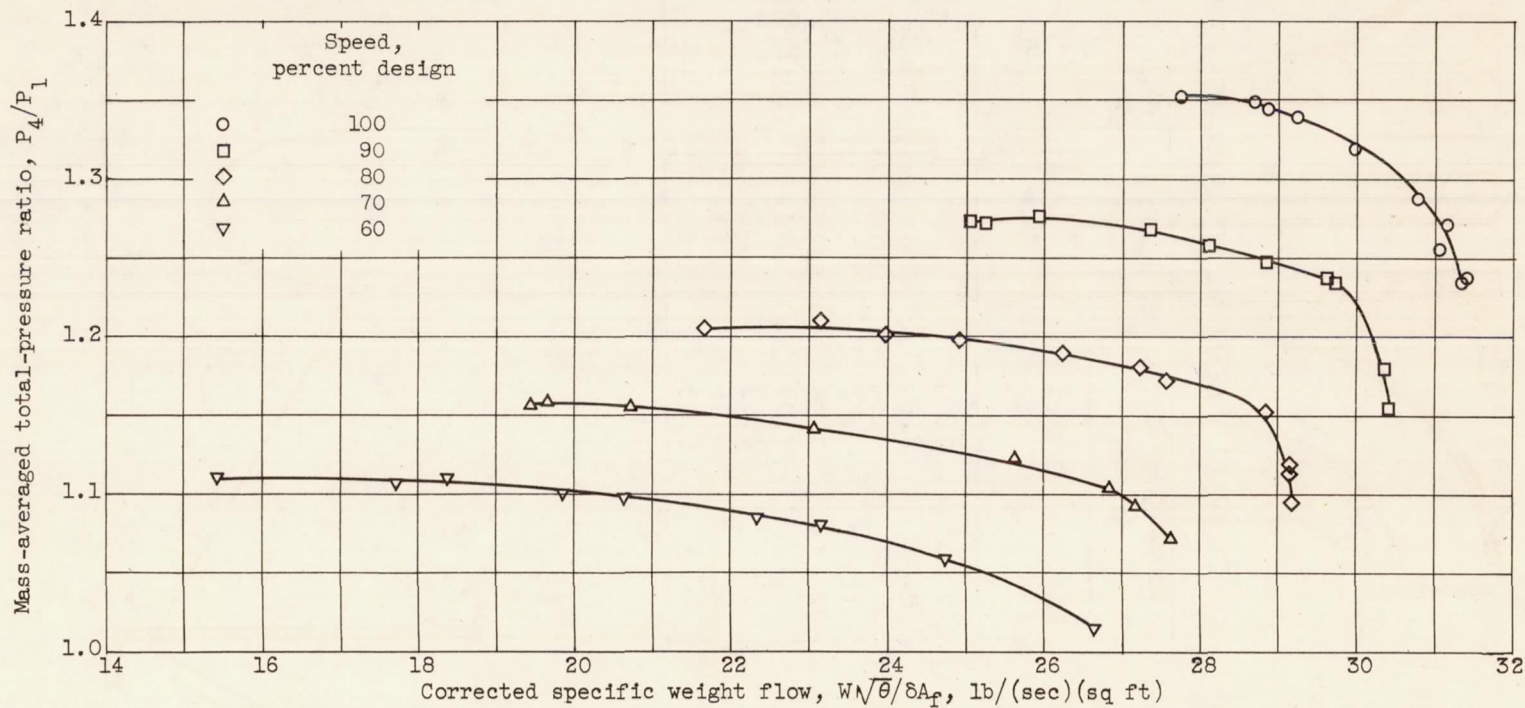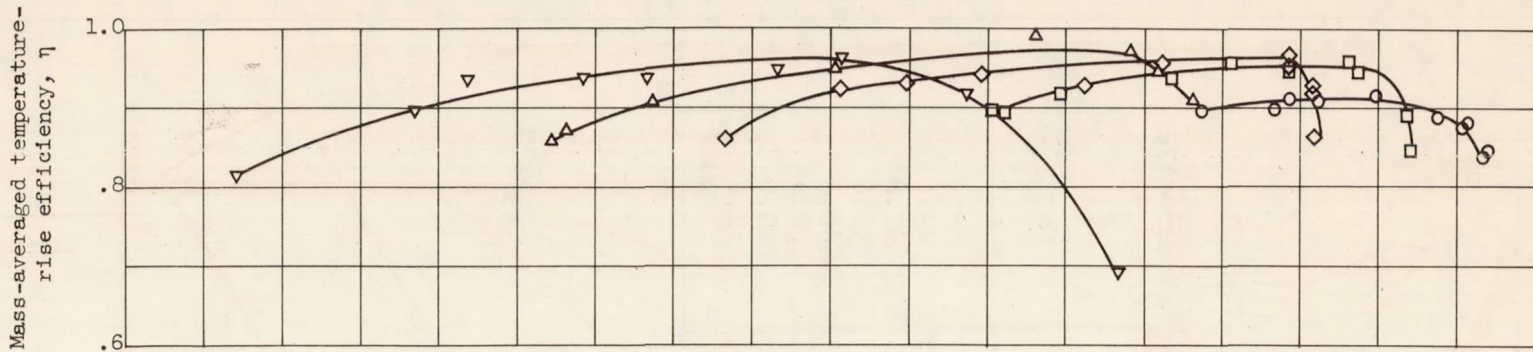
Figure 1. - Mass-averaged performance of 1.5-inch-chord transonic compressor rotor.

Collector

Rotor

Air
flow

Static-
pressure
rake

Station   1

2 3   4

CD-3611
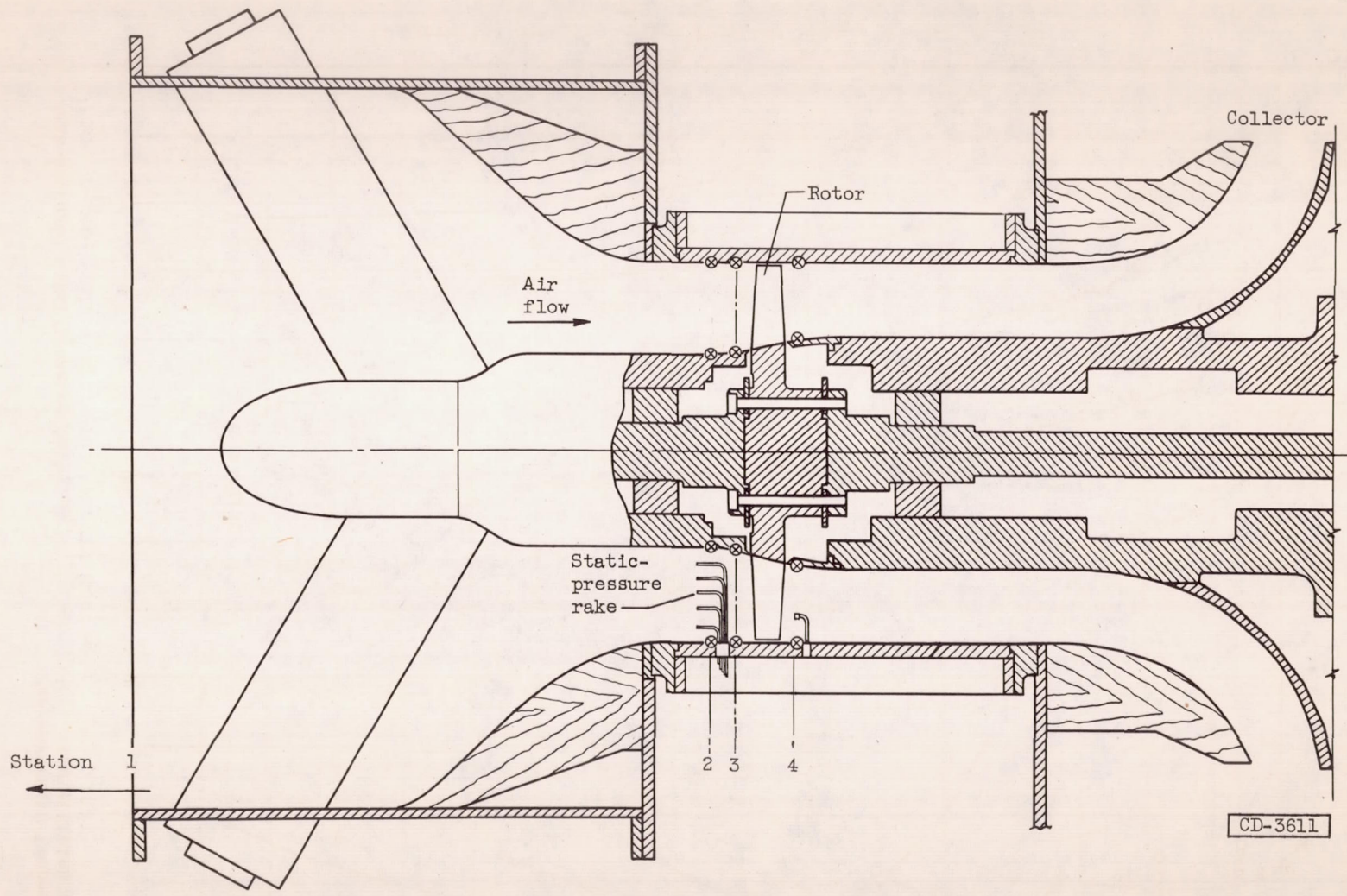
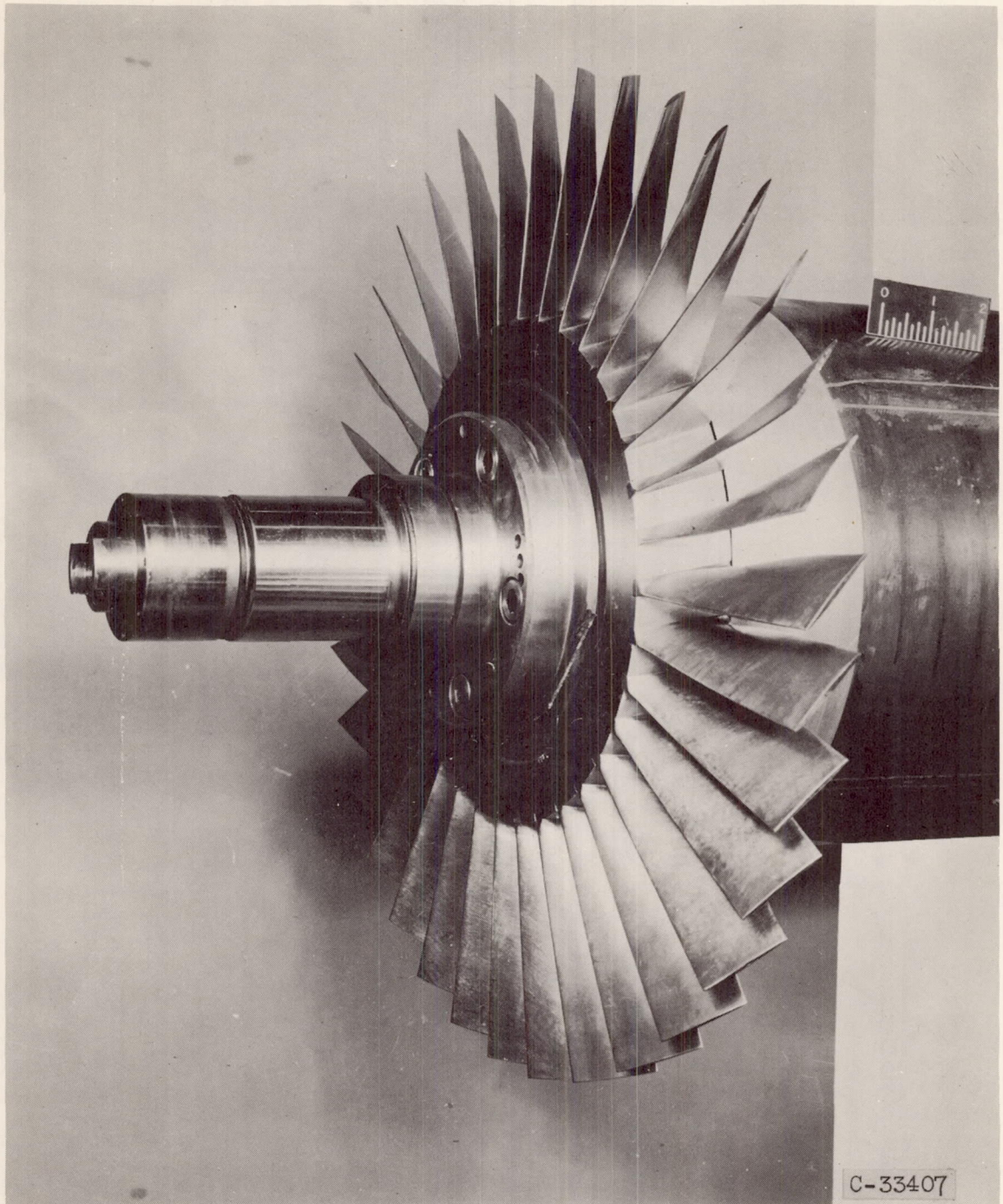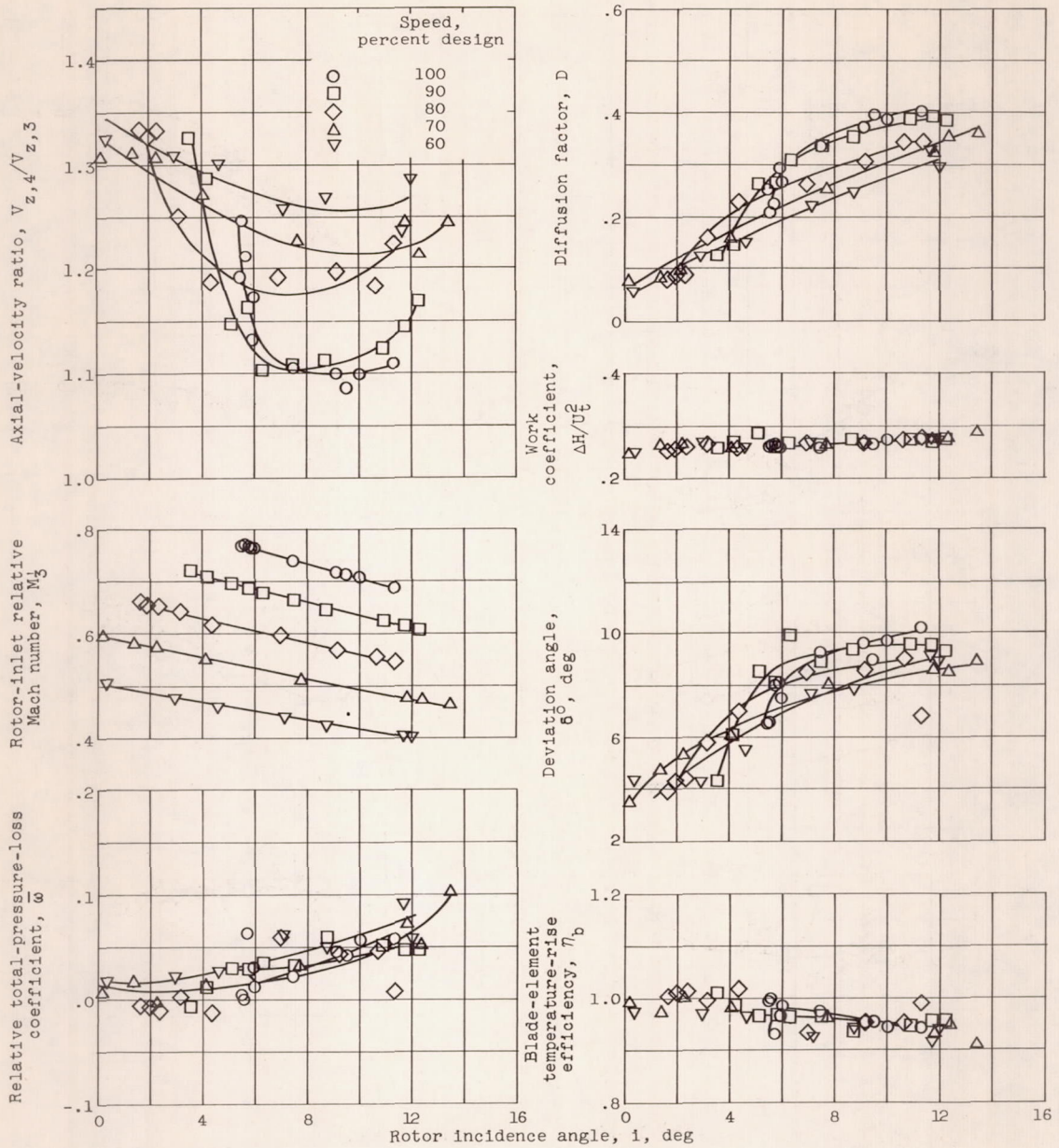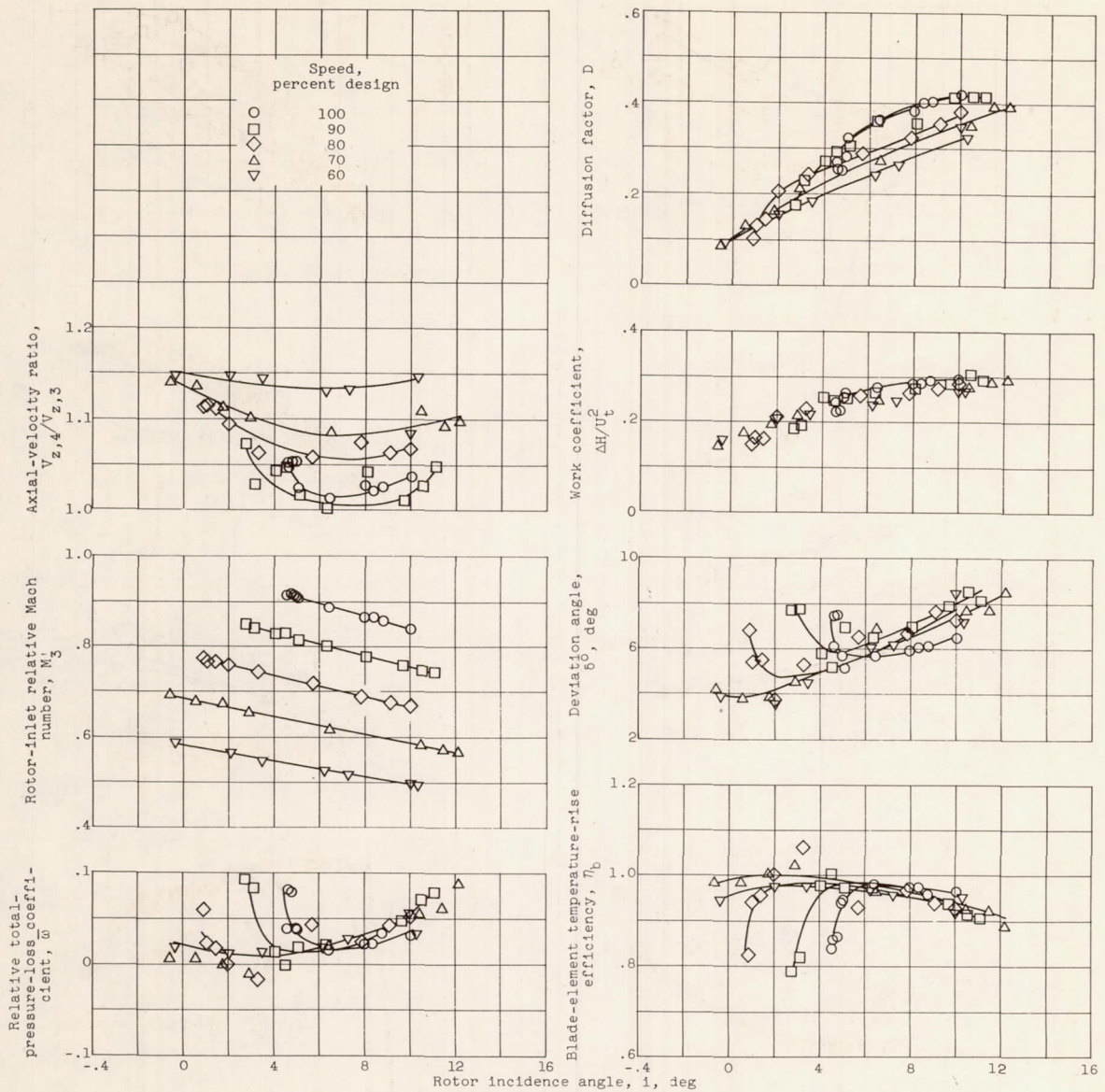Figure 2. - Schematic diagram of variable-component transonic compressor test rig.

Figure 3. - 1.5-Inch-chord transonic compressor rotor.
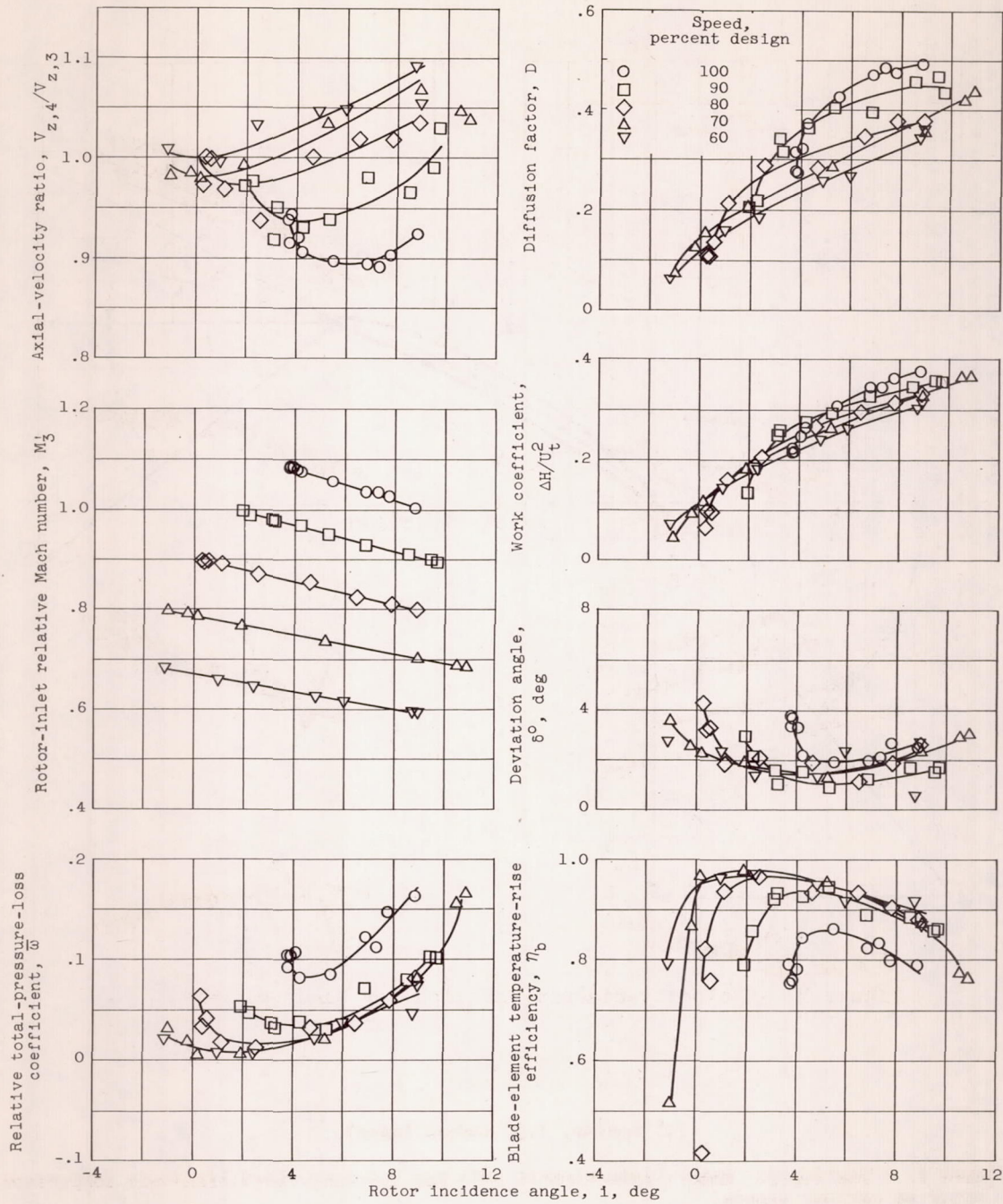
(a) Radius, 5.64 inches (near hub).

Figure 4. – Rotor-blade-element data for 1.5-inch-chord transonic compressor rotor at various speeds.

(b) Radius, 7.00 inches (mean).

Figure 4. - Continued. Rotor-blade-element data for 1.5-inch-chord transonic compressor rotor at various speeds.

(c) Radius, 8.60 inches (near tip).

Figure 4. - Concluded. Rotor-blade-element data for 1.5-inch-chord transonic compressor
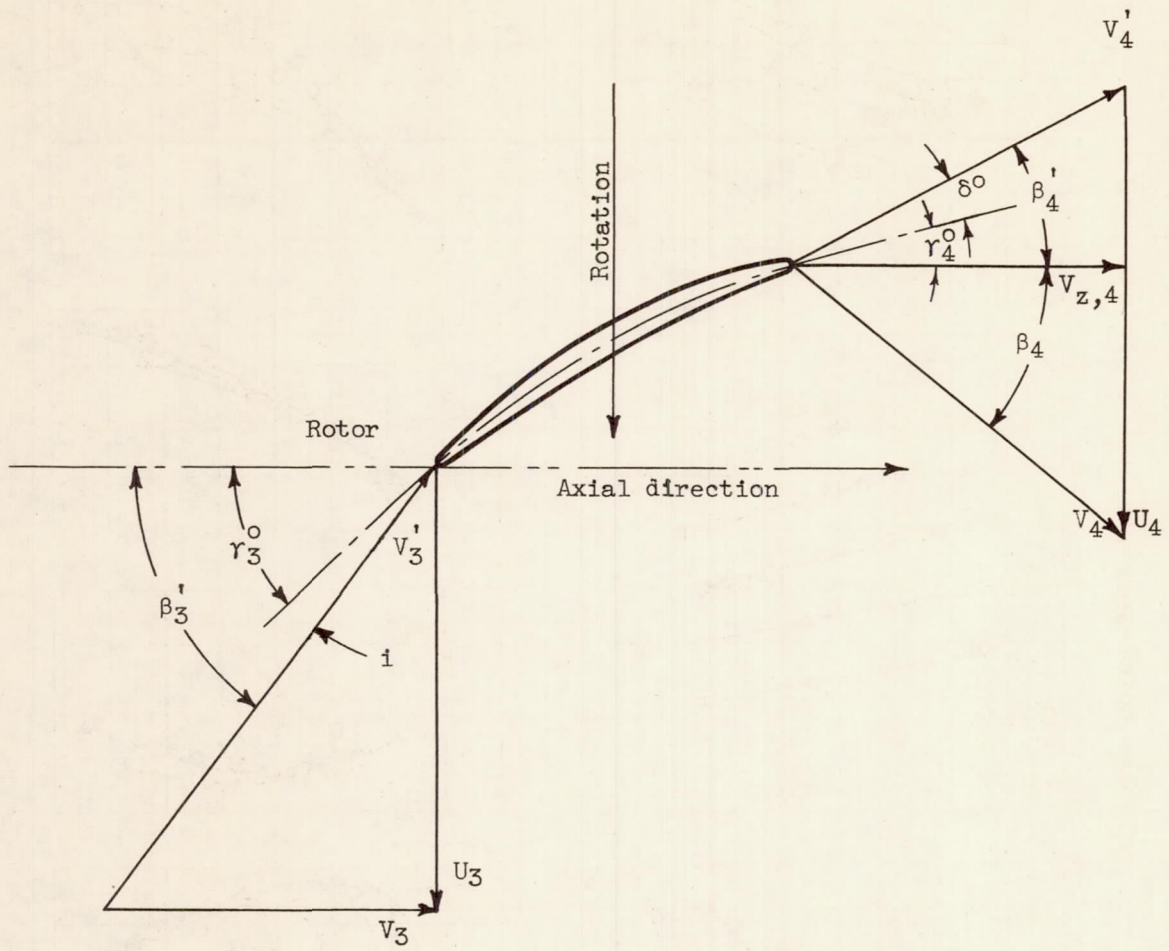   rotor at various speeds.

3693

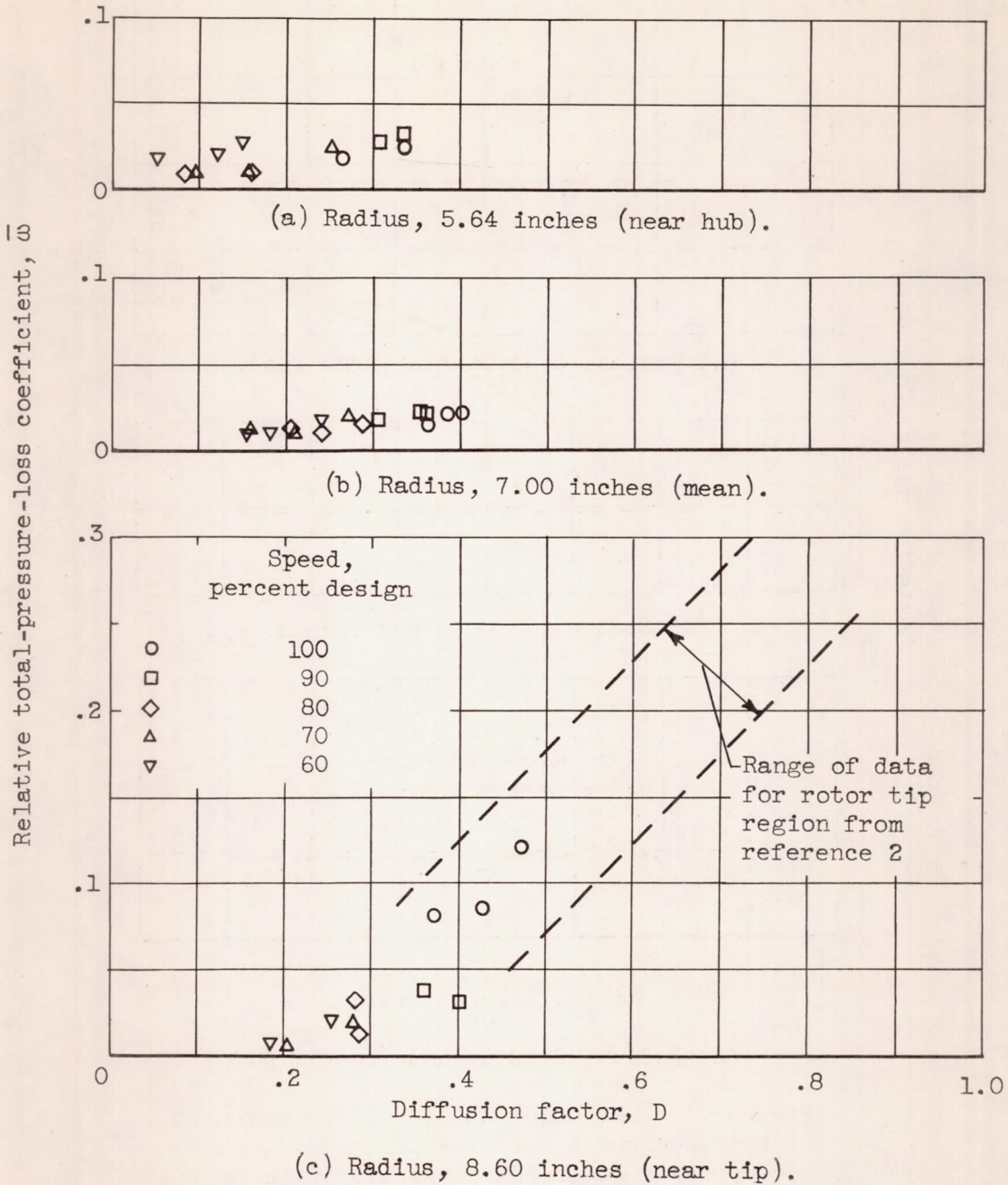Figure 5. - Velocity-diagram notation for blade element.

(a) Radius, 5.64 inches (near hub).

(b) Radius, 7.00 inches (mean).

Speed,
percent design

○	100
□	90
◇	80
△	70
▽	60

Range of data
for rotor tip
region from
reference 2

Diffusion factor, D

(c) Radius, 8.60 inches (near tip).

Figure 6. - Variation of rotor-blade-element losses with diffusion factor in low-loss range of incidence angle.

3693

(a) Radius, 5.64 inches (near hub).

(b) Radius, 7.00 inches (mean).

o   Measured values
— — —Carter's rule

Speed, percent design
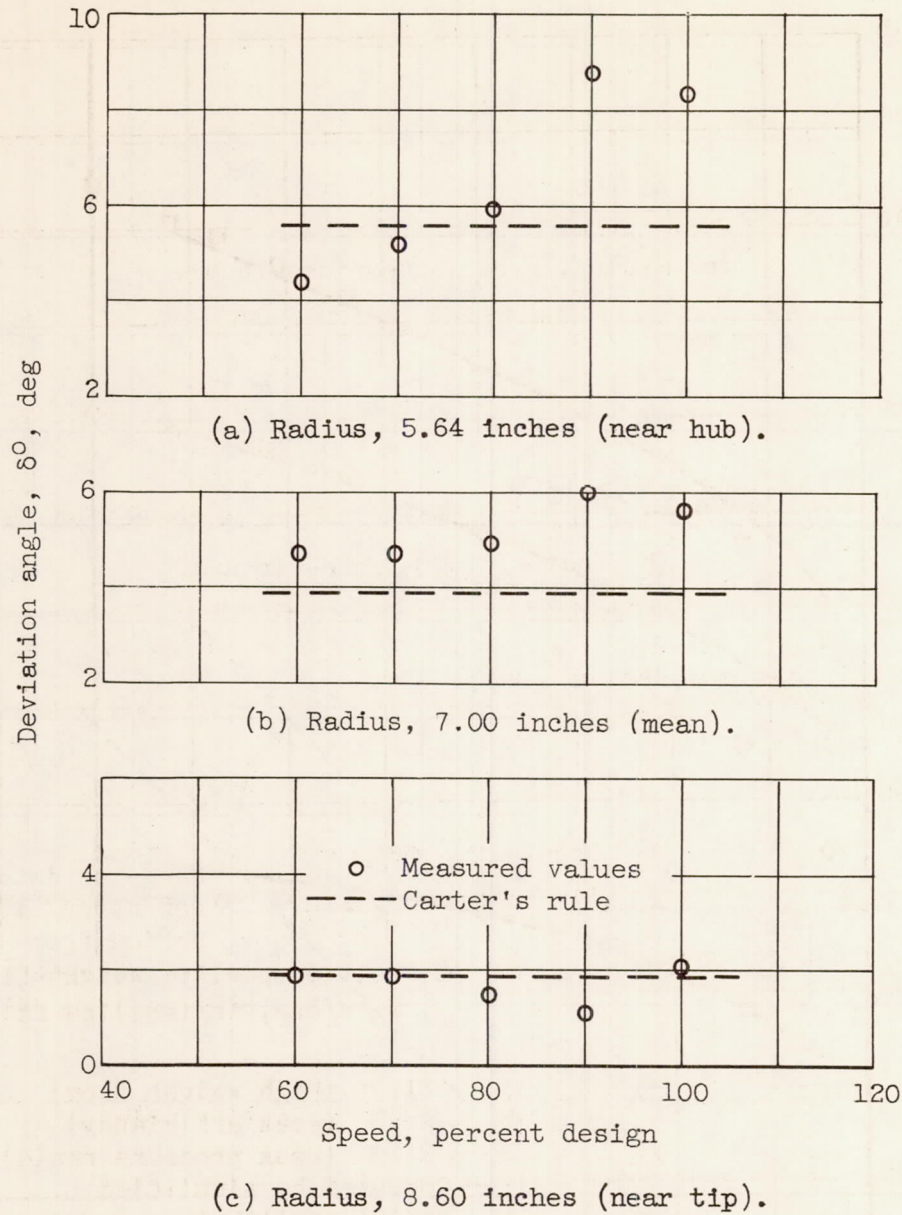
(c) Radius, 8.60 inches (near tip).

Figure 7. - Deviation angles at minimum-loss
incidence angle for 1.5-inch-chord transonic
compressor rotor and comparison with values
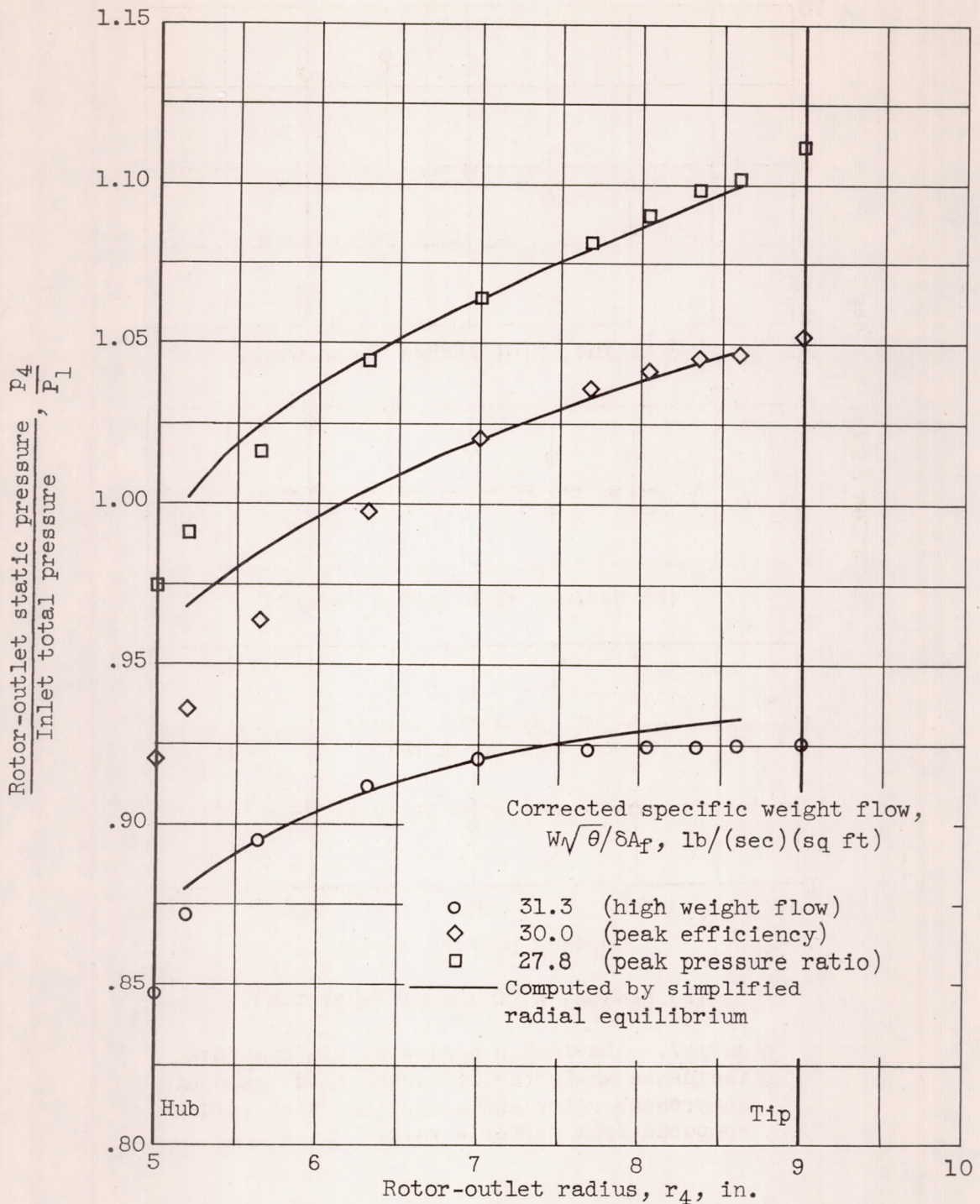computed from Carter's rule.

3693

Figure 8. - Comparison between rotor-outlet static pressures
(survey) and static pressures computed by assuming simpli-
fied radial equilibrium at design speed.